LETTERS IN BIOMATHEMATICS
An International Journal

Intercollegiate Biomathematics Alliance

RESEARCH ARTICLE

OPEN ACCESS

Adaptive Social Distancing Strategies for Controlling Infection Inequality in Emerging Infectious Diseases

Asma Azizi[a], Caner Kazanci[b,c], Sunmi Lee[d]

[a]Department of Mathematics, Kennesaw State University, Marietta, GA 30060; [b]Department of Mathematics, University of Georgia, Athens, GA 30602; [c]College of Engineering, University of Georgia, Athens, GA 30602; [d]Department of Applied Mathematics, Kyung Hee University, Yongin, Republic of Korea

ABSTRACT

People fare in outbreaks of emerging infections based on social factors shaping their exposure and vulnerability to the virus. This different exposure cause a disproportionate share of prevalence among people with various socioeconomic statuses. Therefore, socioeconomic-based control strategies are needed to control the discrepancy in prevalence among socioeconomic groups. We propose and analyze a SIR mathematical model that is grouped based on individuals' income level (representing socioeconomic status). For the model's parameter, we use properties of a real-world social network of individuals residing in New Orleans, Louisiana. We then distribute the social distancing practice among different groups to minimize a multi-objective function of infection characteristics (final epidemic size) and the discrepancy of prevalence among them (infection inequality). Our result confirms the importance of the heterogeneous distribution of social distancing practices among various socioeconomic groups to reduce observed infection inequality. At the same time, it does not considerably impact the final epidemic size.

ARTICLE HISTORY
Received June 21, 2023
Accepted November 16, 2023

KEYWORDS
emerging infection, health disparity, infection inequality, social distancing, mathematical modeling

1 Introduction

The socioeconomically disadvantaged population continues to experience a disproportionate share of emerging infectious diseases. For example, historical accounts of influenza pandemics demonstrated that Low-income people were affected by the 1918 pandemic more than High-income ones in the United States (Sydenstricker, 1931), or the distribution of Ebola outbreaks tied to a particular group of people living in poverty, and health care workers who serve the poor community, but not others in close physical proximity (Farmer, 1996). In the recent pandemic of SARS-Cov-2, people of low socioeconomic status were at high risk of catching the infection because of cramped living conditions, lack of self-isolation, higher rates of many of the comorbidities such as hypertension, and lack of opportunity to work from home that renders them exposed to other individuals at their workplace (Mackenbach et al., 2008; Tjepkema et al., 2013; Álvarez et al., 2011; Anderson et al., 2020; Cardoso et al., 2004). Social factors originating from poverty and social inequalities are linked to many other emerging infectious diseases such as malaria and tuberculosis (Farmer, 1996; Uscher-Pines et al., 2007). Thus, it is crucial to focus on social determinants deriving health inequality in preparedness planning for emerging infections (Quinn and Kumar, 2014). Blumenshine et al. (2008) mentioned the need for systematic and concrete planning to minimize the disparities that can occur in the face of natural disasters, such as emerging infection spread.

Mathematical models are excellent tools for understanding the underlying epidemiology of diseases and how they correlate to the social structure of the infected population (Del Valle et al., 2005, 2007; Hyman and Li, 1997a,b; Hyman et al., 1999, 2001). These models help the medical/scientific community anticipate the spread of diseases and evaluate the potential impact of different approaches, such as Social Distancing (SD), for bringing the epidemic under control. Without any pharmaceutical treatments or vaccines, SD is an effective approach to reducing emerging infection and mortality (Block et al., 2020; Bayham et al., 2015; Desclaux et al., 2017). But it works unevenly across various socioeconomic classes (VoPham et al., 2021) because of many reasons, such as being unable to afford SD by lower socioeconomic classes. During the outbreak, this uneven share of behavior change causes the socioeconomic class to play a key role in the discrepancy in prevalence among various communities,

CONTACT Asma Azizi aazizi@kennesaw.edu

which we have observed and continue observing in many disasters such as the recent pandemic of COVID-19 (Clouston et al., 2021; Zelner et al., 2021; Kamis et al., 2021; Sweeney et al., 2021). Despite the importance of this unsolved issue, limited mathematical models have accounted for the social and structural factors such as socioeconomic classes or race when modeling SD to bring the epidemic under control (Jacquez et al., 1988; Azizi et al., 2016). Zelner et al. (2022) raised the question, "Why do epidemiological models of emerging infections typically ignore known structural drivers of disparate health outcomes?" Related to this question, we raise the main goal of our work under the question, *"How epidemiological models of emerging infections can be used to control infection inequality among different socioeconomic classes?"*

Our focus is to provide an equitable SD strategy to control the infection characteristic and reduce disparities in the burden of emerging infections. We know that mandated SD can change the course of infection. However, our recent work indicates that its implementation method may cause adverse results on disease spread (Azizi et al., 2022) or possible amplification of the health disparity. For instance, School Closure increased the attack rate in the 2009 H1N1 influenza pandemic (Lee et al., 2010; Maharaj and Kleczkowski, 2012). We want to explore a complementary trend: How to distribute the SD effort among various socioeconomic groups to minimize the epidemic and infection inequality responses? To this end and in continuation of our previous work (Azizi et al., 2022; Komarova et al., 2021; Azizi et al., 2020), we propose a Susceptible-Infected-Removed (SIR) group-based model with contact and social characteristic taken from a real-life social network of individuals residing in New Orleans, Louisiana (Eubank et al., 2010; Azizi, 2023; Eubank, 2008). We define the infection inequality by measuring the difference in prevalence in various groups and then use optimization to find the SD distribution that minimizes our objective function, which is a function of infection characteristics and inequality. Given the limited source for mandated SD implementation, its proper management of distributing SD among various socioeconomic groups will enable us to control infection inequality, even if it has yet to have a practical impact on containing infection characteristics.

The structure of our paper is as follows: In Section 2, we develop our model, conduct model analysis, and introduce optimal social distancing problems to control infection inequality. Section 3 provides numerical simulations of the model to compare various social distancing scenarios and their impact on infection inequality. We end the paper by discussing the importance of social distancing distribution management among various socioeconomic classes and how this management can control infection inequality.

2 Method

Assuming a closed steady-state population of N individuals, we stratify it into K different socioeconomic groups. These individuals are in contact and, therefore, cause an infection spread via a Susceptible-Infected-Recovered (SIR) structure, shown in the system (1):

$$\frac{dS_k}{dt} = \mu_k N_k - \sum_{i=1}^{K} \beta_k C_{ki} \frac{I_i}{N_i} S_k - \mu_k S_k, \qquad \frac{dI_k}{dt} = \sum_{i=1}^{K} \beta_k C_{ki} \frac{I_i}{N_i} S_k - (\gamma_k + \mu_k) I_k, \qquad \frac{dR_k}{dt} = \gamma_k I_k - \mu_k R_k, \tag{1}$$

where N_k, S_k, I_k, and R_k are the number of all, susceptible, infectious, and recovered individuals in group k, respectively, for $k \in \{1, \ldots, K\}$. The parameter $\beta_k > 0$ is the probability of transmission per contact for group k, γ_k is the recovery rate for group k, μ_k is the natural birth or death rate for group k, and $C_{kk'}$ is the number of contact between two individuals in groups k and k' per unit time. Let C_k denote the total number of contacts per time for an individual in group k. We first need to ensure that C_k is partitioned among all the groups, and hence, $\sum_{i=1}^{K} C_{ki} = C_k$. Then, we consider the desirability of contact between people in two groups k and k'. That is, if all people in group k make, say, L contacts with all people in group k', then all people in group k' also make the same amount of L contacts with all people in group k. The number of contacts that all individuals in group k make with individuals from group k' is $C_{kk'} N_k$, and the contacts that all individuals in group k' make with individuals from group k is $C_{k'k} N_{k'}$. These two values are equal, and hence, $C_{kk'} N_k = C_{k'k} N_{k'}$.

Defining the $K \times K$ contact matrix $C = (C_{kk'})$, and implementing these two criteria gives us the balanced conditions defined as follows:

$$\sum_{i=1}^{K} C_{ki} = C_k, \qquad C_{kk'} N_k = C_{k'k} N_{k'}. \tag{2}$$

There are various ways to define the elements of matrix C using the balanced condition (2), such as proportional mixing (Nold, 1980) that assumes the mixing is constrained by the activity levels, that is, the number of contacts any group i has with a typical group j is proportional to the relative activity levels of group j, $C_{ij} = \frac{C_j}{\sum_k C_k}$. Here, we use a real social network of contacts, so the matrix C is entirely well-defined.

2.1 Model analysis

Definition 1 (Connected groups). We say two groups k and k' are connected if there is at least one contact between their members, that is, $C_{kk'} > 0$ and, therefore, $C_{k'k} > 0$.

Theorem 2.1. *The connected groups have the same behavior:*

(a) If the system is at equilibrium and there is no disease in group k, then there is no disease in all the other connected groups k′.

(b) If the system is at equilibrium and group k is at endemic state, then the disease is at endemic for all the other connected groups k′.

Proof. (a) Because the system is at equilibrium and there is no infection in group k, then, $I_k = 0$, also $\frac{dI_k}{dt} = 0$, thus

$$0 = \sum_{i=1}^{K} \beta_k C_{ki} \frac{I_i}{N_i} S_k - (\gamma_k + \mu_k) I_k = \sum_{i=1}^{K} \beta_k C_{ki} \frac{I_i}{N_i} S_k.$$

Because all terms in the summation above are non-negative, all terms—including the k'-th term—should be equal to zero; therefore, $\beta_k C_{kk'} \frac{I_{k'}}{N_{k'}} S_k = 0$. At equilibrium $S_k \neq 0$, because

$$\frac{dS_k}{dt} = \mu_k N_k - \sum_{i=1}^{K} \beta_k C_{ki} \frac{I_i}{N_i} S_k - \mu_k S_k = 0,$$

thus,

$$\mu_k N_k - \left(\sum_{i=1}^{K} \beta_k C_{ki} \frac{I_i}{N_i} + \mu_k \right) S_k = 0.$$

Then, solving the equation for S_k, we have

$$S_k = \frac{\mu_k N_k}{\beta_k \sum_{i=1}^{K} C_{ki} \frac{I_i}{N_i} + \mu_k} \neq 0.$$

Hence, $\beta_k C_{kk'} \frac{I_{k'}}{N_{k'}} = 0$, The non-negativity of parameters guarantees $\beta_k > 0$ and because the groups k and k' are connected $C_{kk'} > 0$, thus, $I_{k'} = 0$.

(b) When the system is at equilibrium and is endemic at group k, then $I_k > 0$. Suppose there is a group k' connected to group k such that $I_{k'} = 0$ therefore,

$$0 = \frac{dI_{k'}}{dt} = \sum_{i=1}^{K} \beta_{k'} C_{k'i} \frac{I_i}{N_i} S_{k'} - (\gamma_{k'} + \mu_{k'}) I_{k'} = \sum_{i=1}^{K} \beta_{k'} C_{k'i} \frac{I_i}{N_i} S_{k'}$$

Because all terms in the summation above are non-negative, all terms—including the k-th term—should be zero, then we have $\beta_{k'} C_{k'k} \frac{I_k}{N_k} S_{k'} = 0$. Because of the same reasoning in part (a), at equilibrium $S_{k'} = \frac{\mu_{k'} N_{k'}}{\beta_{k'} \sum_i C_{k'i} \frac{I_i}{N_i} + \mu_{k'}} \neq 0$. Also, because of the positivity of parameters $\beta_{k'} > 0$ and because groups k and k' are connected $C_{k'k} > 0$, we have that $I_k = 0$ which contradicts the assumption of the theorem. We conclude that $I_{k'} > 0$ for all $k' = 1, \ldots, K$. □

We rewrite our model in matrix form to calculate the basic reproduction number of the model denoted by $\mathcal{R}_0$ and the final epidemic size relation. We define $\vec{S} = [S_1, \ldots, S_K]^T$, $\vec{I} = [I_1, \ldots, I_K]^T$, $\vec{R} = [R_1, \ldots, R_K]^T$, $\vec{N} = [N_1, \ldots, N_K]^T$, $\vec{\beta} = [\beta_1, \ldots, \beta_K]^T$, $\vec{\gamma} = [\gamma_1, \ldots, \gamma_K]^T$, and $\vec{\mu} = [\mu_1, \ldots, \mu_K]^T$. We can rewrite the system (1) as a matrix form

$$\begin{aligned} \frac{d\vec{S}}{dt} &= D(\vec{\mu})\vec{N} - D(\vec{S})D(\vec{\beta})CD(\vec{N})^{-1}\vec{I} - D(\vec{\mu})\vec{S}, \\ \frac{d\vec{I}}{dt} &= D(\vec{S})D(\vec{\beta})CD(\vec{N})^{-1}\vec{I} - D(\vec{\gamma} + \vec{\mu})\vec{I}, \\ \frac{d\vec{R}}{dt} &= D(\vec{\gamma})\vec{I} - D(\vec{\mu})\vec{R}, \end{aligned} \tag{3}$$

where the operator $D(\vec{x})$ is a diagonal matrix with $D(i,i) = x_i, 1 \leq i \leq K$.

Basic reproduction number. The basic reproduction number $\mathcal{R}_0$ is one characteristic of an epidemic that measures the number of people a typical infected individual can infect at the early stage of the epidemic when almost all population is susceptible. Since there are a few infected individuals and no recovered ones at the early stage of the epidemic, it is reasonable to assume almost all of the population is susceptible at the early stage, that is, $\vec{S} \approx \vec{N}$. Doing so, we can rewrite the infection state of the system (3) as

$$\frac{d\vec{I}}{dt} \approx J\vec{I},$$

where

$$J = -D(\vec{\gamma} + \vec{\mu}) + D(\vec{N})D(\vec{\beta})CD(\vec{N})^{-1}.$$

Case 1: In the simplest homogeneous case, we assume all groups are connected and all groups' transmission, recovery, and birth/death rates are identical. Namely $C_{ij} > 0$ for all i and j, $\beta_k = \beta$, $\gamma_k = \gamma$, and $\mu_k = \mu$ for $k = 1, \ldots, K$. Without loss of generality, we re-scale time by $\gamma + \mu$, then

$$J = -D(\vec{1}) + \frac{\beta}{\gamma + \mu}B,$$

where $D(\vec{1})$ is identity matrix and $B = D(\vec{N})CD(\vec{N})^{-1}$. We use $\lambda_{\max}(A)$ to represent the largest real part of the eigenvalue of a typical matrix A. The disease Free Equilibrium (DFE), where $\vec{I} = \vec{0}$, is stable when $\lambda_{\max}(J) = -1 + \frac{\beta}{\gamma+\mu}\lambda_{\max}(B) < 0$. Obviously, $\lambda_{\max}(B) = \lambda_{\max}(C)$. Then, the stability of DFE corresponds to the condition $-1 + \frac{\beta}{\gamma+\mu}\lambda_{\max}(C) < 0$; otherwise, the Endemic Equilibrium (EE) is stable. The condition $-1 + \frac{\beta}{\gamma+\mu}\lambda_{\max}(C) < 0$ is equivalent to $\frac{\beta}{\gamma+\mu}\lambda_{\max}(C) < 1$. This proves that the basic reproduction number of model is

$$\mathcal{R}_0 = \frac{\beta}{\gamma + \mu}\lambda_{\max}(C).$$

Case 2: For the general case when groups are heterogeneous in terms of infection propagation, that is, when $\beta_k \neq \beta_{k'}$, $\gamma_k \neq \gamma_{k'}$, and $\mu_k \neq \mu_{k'}$ for at least a pair of k and k', for $k, k' = 1, \ldots, K$, then the next generation matrix calculated through next-generation approach (Van den Driessche and Watmough, 2002) is

$$X = D(\vec{N})D(\vec{\beta})CD(\vec{N})^{-1}D(\vec{\gamma} + \vec{\mu})^{-1}. \tag{4}$$

The $\mathcal{R}_0$ for the whole system is spectral radius of matrix X, $\rho(X)$. But our goal is to dig into elements of matrix X to understand their meanings. That way, we can know about appropriate ways to control infection in the system. Each element X is given as

$$X(i,j) = \beta_i C_{ij}\frac{N_i}{N_j}\frac{1}{\gamma_j + \mu_j}, \tag{5}$$

By balanced condition $C_{ij}\frac{N_i}{N_j} = C_{ji}$, therefore,

$$\begin{aligned} X(i,j) &= \begin{pmatrix}\text{Probability of disease}\\ \text{transmission in group } i\end{pmatrix}\begin{pmatrix}\text{Number of contacts a person in}\\ \text{group } j \text{ makes with people in group } i\end{pmatrix}\begin{pmatrix}\text{Infection period for infected}\\ \text{and alive person in group } j\end{pmatrix} \\ &= \qquad \beta_i \qquad\qquad\qquad C_{ji} \qquad\qquad\qquad \frac{1}{\gamma_j + \mu_j}. \end{aligned}$$

We denote element $X(i,j)$ by $\mathcal{R}_0^{j\to i}$ as the number of people in group i where get infected by an individual in group j (Diekmann et al., 2010; Hartemink et al., 2008). For example, the diagonal element of matrix X, $X(i,i) = \mathcal{R}_0^{i\to i}$, is the average number of infected cases belonging to group i produced by a typical infected individual belonging to the same group i. We call this value $\mathcal{R}_0^{i\to i}$ the basic reproduction of group i.

Final size relation. Using (Arino et al., 2007), we have final size relation

$$\ln\left(\frac{\vec{S}_0}{\vec{N} - \vec{R}_\infty}\right) = D(\vec{\beta})CD(\vec{N})^{-1}D(\vec{\gamma} + \vec{\mu})^{-1}\vec{R}_\infty = D(\vec{N})^{-1}X\vec{R}_\infty, \tag{6}$$

where logarithmic function and fraction on the left-hand side of equation (6) operate element by element, $\vec{R}_\infty$ is the vector of recovered individuals at final time, when t approaches to ∞, and $\vec{S}_0$ is the vector of susceptible individuals at the initial time.

The k-th component of vector form (6) is

$$\ln\left(\frac{S_{k0}}{N_k - R_{k\infty}}\right) = \sum_j \beta_k C_{kj} \frac{R_{j\infty}}{N_j(\gamma_j + \mu_j)} = \frac{1}{N_k}\sum_j \mathcal{R}_0^{j\to k} R_{j\infty}, \qquad k = 1, \ldots, K, \tag{7}$$

where $R_{k\infty}$ is the k-th element of $\vec{R}_\infty$, and S_{k0} is the k-th element of $\vec{S}_0$. We note that the balanced condition $C_{kj}N_k = C_{jk}N_j$ is used to derive the second equality in the equation in (7). Equation (7) implies that the final size $R_{k\infty}$ of group k is an increasing function of the final size $R_{j\infty}$ of other groups j that are connected to k ($C_{kj} \neq 0$.) Thus, the final size of group k can be controlled by the the final sizes of connected groups j via interventions.

Theorem 2.2. *Suppose the reproduction for group k is less than one, that is, $\mathcal{R}_0^{k\to k} < 1$. Then reducing the final size $R_{k'\infty}$ for group k' connected to group k causes a reduction of the final size for group k.*

Proof. Without loss of generality, we assume that we have only two groups called k and k'. Then by (7) we have

$$R_{k\infty} = N_k - S_{k0}e^{-\frac{1}{N_k}(\mathcal{R}_0^{k\to k}R_{k\infty} + \mathcal{R}_0^{k'\to k}R_{k'\infty})}$$

Dividing both side of equation by N_k and then defining continuous variables $x = \frac{R_{k'\infty}}{N_{k'}} \in [0,1]$ and $y = \frac{R_{k\infty}}{N_k} \in [0,1]$, we have

$$y = 1 - \frac{S_{k0}}{N_k}e^{-(\mathcal{R}_0^{k\to k}y + \frac{N_{k'}}{N_k}\mathcal{R}_0^{k'\to k}x)}$$

Taking the derivative of both sides with respect to x, we have

$$\begin{aligned}
\frac{dy}{dx} &= \frac{S_{k0}}{N_k}(\mathcal{R}_0^{k\to k}\frac{dy}{dx} + \frac{N_{k'}}{N_k}\mathcal{R}_0^{k'\to k})e^{-(\mathcal{R}_0^{k\to k}y + \frac{N_{k'}}{N_k}\mathcal{R}_0^{k'\to k}x)} \\
&= \frac{S_{k0}}{N_k}(\mathcal{R}_0^{k\to k}\frac{dy}{dx} + \frac{N_{k'}}{N_k}\mathcal{R}_0^{k'\to k})\frac{N_k}{S_{k0}}(1-y) \\
&= (\mathcal{R}_0^{k\to k}\frac{dy}{dx} + \frac{N_{k'}}{N_k}\mathcal{R}_0^{k'\to k})(1-y).
\end{aligned}$$

Therefore,

$$[1 - \mathcal{R}_0^{k\to k}(1-y)]\frac{dy}{dx} = \frac{N_{k'}}{N_k}\mathcal{R}_0^{k'\to k}(1-y).$$

We note that the R.H.S. of the above equation is always non-negative. On the other hand, by the assumptions $\mathcal{R}_0^{k\to k} \leq 1$ and $y \in [0,1]$, it can be shown that $1 - \mathcal{R}_0^{k\to k}(1-y) \geq 0$. That results in $\frac{dy}{dx} \geq 0$, which proves our theorem. □

The basic reproduction number of the whole system, $\mathcal{R}_0$, is a function of all $R_0^{i\to j}$ for all i and j, as it is the spectral radius of the matrix X whose elements are $R_0^{i\to j}$. Therefore, even if the basic reproduction number of group k is less than one, $R_0^{k\to k} < 1$, group k still can experience an outbreak if $\mathcal{R}_0 > 1$. However, based on the theorem above, we can control the epidemic (reduce the final size) in group k by implementing Non-Pharmaceutical Intervention (NPI) such as SD on another connected group k'. On the other hand, if the reproduction of group k is so big that causes that $\mathcal{R}_0^{k\to k}(1-y) = \mathcal{R}_0^{k\to k}\frac{S_{k\infty}}{N_k} > 1$, then, implementing an NPI to control the final size of a connected group k' results in increasing final size for group k.

2.2 Social distancing and infection inequality

In mandated SD, the decrease in social contacts is regulated centrally and affects the entire population or specific subpopulations (Glass et al., 2006; Valdez et al., 2012). To this end, if the level of mandated SD is $\sigma \in [0,1]$, then the level of contact is reduced by σ. We assume an individual in group k practices SD with level $\sigma_k \in [0,1]$. Thus, a person in group k reduces contact from C_k to $(1-\sigma_k)C_k$. Doing so, the second equation in balance conditions (2) will change to

$$(1-\sigma_k)C_{kk'}N_k = (1-\sigma_{k'})C_{k'k}N_{k'}.$$

We assume the given parameter $\sigma \in [0,1]$ is the SD level for the whole population, that is, if average contact for all population is $\bar{C} = \frac{\sum_{k=1}^K C_k N_k}{N}$, where $N = \sum_k N_k$ is total population size, then all population practice SD by reducing the contact level to $(1-\sigma)\bar{C}$. Then, the question is how to distribute σ over the groups. In other words, if σ_k is level of SD for group $k = 1, 2, \ldots, K$, then given σ how can we specify σ_k. To answer this question, we first need to define an objective function related to infection

characteristics and infection inequality. The infection inequality is defined so that differences in prevalence in all groups are minimized. If we define $i_k(t) = \frac{I_k(t)}{N_k}$ as fraction of infected individuals in group k at time t, then we define

$$\mathcal{D}(t) = \sum_{\substack{k,k' \\ k<k'}} |i_k(t) - i_{k'}(t)|, \qquad \mathcal{D}_T = \int_0^T \mathcal{D}(t)dt. \tag{8}$$

$\mathcal{D}(t)$ is called infection inequality at time t, and $\mathcal{D}_T$ is the total infection inequality defined in the whole infection time frame $[0, T]$. On the other hand, suppose $r_\infty = \frac{R_\infty}{N} = \frac{\sum_k R_{k\infty}}{N}$ is final size fraction of the population, fraction of all people who got infected at some time during the infection spread, which is measured by the number of recovered people at final time divided by population size. Therefore, our optimization problem is stated as

$$\min_{\sigma_1,\dots,\sigma_K} \Lambda_\alpha = \alpha\mathcal{D}_T + (1-\alpha)r_\infty \qquad \text{s.t.} \quad \sum_{k=1}^{K} \sigma_k C_k N_k = \sigma \bar{C} N \qquad 0 \le \sigma_k \le 1, \text{ for } k = 1,\dots,K \tag{9}$$

where again $\bar{C} = \frac{\sum_{k=1}^{K} C_k N_k}{N}$ is the average contact of the whole population before any SD implementation, and the weight $\alpha \in [0,1]$ is an indicator of the importance of controlling total infection inequality ($\mathcal{D}_T$) over controlling final epidemic size (r_∞); smaller α, more focus on reducing r_∞, and bigger α, more focus on reducing $\mathcal{D}_T$. We solve the problem by finding optimal SD strategy $(\sigma_1^*, \sigma_2^*, \dots, \sigma_K^*)$ that minimizes function $\Lambda_\alpha = \alpha\mathcal{D}_T + (1-\alpha)r_\infty$. The constraint in the optimized problem means that the sum of the total number of contact reduction of group k as a result of σ_k SD implementation should be equal to the total number of contact reduction as a result of σ SD implementation in the whole population. We note that this constraint means compliance with SD is mandated, and the budget for implementing mandated SD is limited. Therefore, based on the model assumption, if one group practices SD weakly, the other has to practice it more strongly. Thus, the focus is to manage the SD effort distribution to our best benefit, minimizing Λ_α.

3 Result

3.1 Parameter value

The definitions of parameters of the proposed model and their baseline values are given in the Table 1. To find contact parameters, we used a social network based on the synthetic data generated by *Simfrastructure*, a high-performance, service-oriented, agent-based modeling and simulation system for representing functioning virtual cities. Simfrastructure represents entire urban populations at the level of individuals, including their activities, movements, and locations, on a second-by-second basis. The data that we used was generated by researchers at Biocomplexity Institute at Virginia Tech (Eubank et al., 2010; Eubank, 2008), and technical report (Azizi, 2023), that are publicly available on GitHub (Azizi, 2023). The data is in the form of a social network of $N \sim 150{,}000$ synthetic people as nodes of the network. Each edge ij between two nodes i and j shows contact between two corresponding individuals and is weighted by some label that reflects the type of connection (Household, Work, School, Shopping, and Others, such as entertainment gatherings or religious activities) as well as the amount of time the two individuals spend with each other. The minimum duration of all contact types is 15 minutes, enough time to spread emerging infections such as COVID-19 (Keeling et al., 2020). The X- and Y-coordinate of household location and per year household income of each individual in the network is given. In Figure 1, we have plotted the income distribution based on the household location of individuals (left panel) and contact probability as a function of household dimensionless distances (right panel). This plot shows that individuals cluster based on their income and have mostly contact with (physically) close people; that is, the chance of contact between two individuals decreases as their household physical distance increases. The plot reveals some correlation between income and contacts. To measure this correlation, we divided the population into three groups: Low-income, Middle-income, and High-income. Individuals with per year household income less than \$48000 are considered as Low-income (57% of the whole population), the ones with per year household income within the range [\$48000, \$145500] are Middle-income (32% of the whole population), and the ones with per year household income higher than \$145500 are High-income (10% of whole population) (Snider and Kerr, 2023). Incorporating this class stratification, we can find contact matrix as follows: for every individual in group $i \in \{\text{L (Low-income), M (Middle-income), H (High-income)}\}$ we count their number of contacts which are in class $j \in \{\text{L, M, H}\}$, lets call it c_{ij}. Then C_{ij} is the average of all the values c_{ij} for all individuals in group i. Using this approach, we found C_{LL}, C_{LM}, C_{LH}, C_{ML} and C_{MM}. For the rest elements of contact matrix (C_{MM}, C_{MH}, C_{HL}, C_{HM}, and

Table 1: Parameters' notations, definitions, units, and baseline values. The values with ∗ sign were rounded up to two digits for reporting in the table.

Contact Parameters		
Notation	Description	Baseline Value (Unit)
N	Number of people	154,240 (People)
N_L	Number of Low-income people	88,445 (People)
N_M	Number of Middle-income people	48,946 (People)
N_H	Number of High-income people	16,849 People
C_L	Contact numbers for a Low-income individual per unit time	12.11 (Contacts/Day)
C_M	Contact numbers for a Middle-income individual per unit time	10.91 (Contacts/Day)
C_H	Contact numbers for a High-income individual per unit time	8.06 (Contacts/Day)
C_{LL}	Contact numbers between two Low-income individuals per unit time	7.40* (Contacts/Day)
C_{LM}	Contact numbers a Low-income individual makes with Middle-income ones per unit time	3.63* (Contacts/Day)
C_{LH}	Contact numbers a Low-income individual makes with High-income ones per unit time	1.07* (Contacts/Day)
C_{ML}	Contact numbers a Middle-income individual makes with Low-income ones per unit time	6.57* (Contacts/Day)
C_{MM}	Contact numbers between two Middle-income individuals per unit time	4.08* (Contacts/Day)
C_{MH}	Contact numbers a Middle-income individual makes with High-income ones per unit time	0.26* (Contacts/Day)
C_{HL}	Contact numbers a High-income individual makes with Low-income ones per unit time	5.64* (Contacts/Day)
C_{HM}	Contact numbers a High-income individual makes with Middle-income ones per unit time	0.75* (Contacts/Day)
C_{HH}	Contact numbers between two High-income individuals per unit time	1.67* (Contacts/Day)
Infection and Intervention Paramters		
Notation	Description	Baseline Value (Unit)
β	Prob. of transmission per contact	0.033 (1/Contact)
$\rho = \gamma + \mu$	Removal (death or recovery) rate	0.1 (1/Day)
σ	Fraction of contacts that are cut by all population	Changing value (1)
σ_L	Fraction of contacts that are cut by Low-income individuals	Changing value (1)
σ_M	Fraction of contacts that are cut by Middle-income individuals	Changing value (1)
σ_H	Fraction of contacts that are cut by High-income individuals due to SD	Changing value (1)
α	Optimization parameter	0.5 (1)

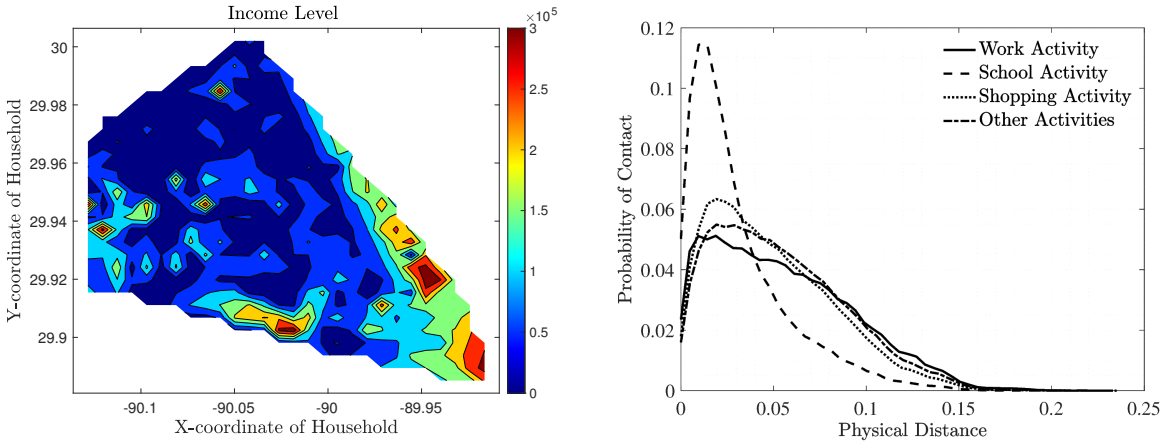

Figure 1: The map of the household location, income level (left panel), and probability of contact as a function of household distance (right panel). Low- (high-) income individuals live in clusters in the same neighborhood. Individuals are primarily in (any type of) physical contact with others nearby.

C_{HH}), we use the balanced condition (2). Below is the result matrix C:

$$C = \begin{array}{r} \\ \text{Low-income} \\ \text{Middle-income} \\ \text{High-income} \end{array} \begin{array}{c} \begin{array}{ccc} \text{Low-income} & \text{Middle-income} & \text{High-income} \end{array} \\ \begin{bmatrix} 7.40 & 3.63 & 1.07 \\ 6.57 & 4.08 & 0.26 \\ 5.64 & 0.75 & 1.67 \end{bmatrix} \end{array}.$$

The total average number of contacts per day for group i is the sum of the contact matrix's i-th row. We observe that the connectivity level of individuals inversely correlates with their socioeconomic status; the average number of contacts per day for a person in the Low-income group is the highest, $C_L = 12.11$, followed by that of the Middle-income, $C_M = 10.91$, and the lowest belongs to High-income group, $C_H = 8.06$. Although the contact matrix is not diagonally dominant, if we scale it by population sizes of groups (dividing each column j by the population size of group j), we observe that the result matrix becomes diagonally dominant, which means a strong assortativity in socioeconomic status; people are better connected to others of their socioeconomic class than to others (Leo et al., 2016).

The infection-related parameter values, such as transmission probability per contact and recovery rate reported in Table 1, have been chosen similarly for all groups and are realistic for respiratory infections such as COVID-19. Recovery rate for COVID-19 was estimated to be around 0.1 (Yang et al., 2021), and $\mathcal{R}_0$ was estimated in the range from 1.5 to 6.49, with an average of 4.2 (Cao et al., 2020; Tang et al., 2020). Therefore, assuming the $\mathcal{R}_0$ without any SD implementation to be around 4, we calculated the transmission rate accordingly. With the baseline values reported in Table 1, we have $\mathcal{R}_0 = 3.77$, basic reproduction number for Low-income group $\mathcal{R}_0^{1\to1} = 2.44$, basic reproduction number for Middle-income group $\mathcal{R}_0^{1\to1} = 1.35$, and basic reproduction number for High-income group $\mathcal{R}_0^{1\to1} = 0.55$.

3.2 Social distancing distribution

Using the global sensitivity analysis on SD parameters σ_L, σ_M, we explore the potential impact of SD distribution on Λ_α reduction. We navigate the (σ_L, σ_M) parameter space for $\sigma_L \in [0, 0.99]$ and $\sigma_M \in [0, 0.99]$ with a step-size of 0.001 and choose the (σ_L, σ_M) pair that minimizes Λ_α. Figure 2 gives the prediction of the Λ_α for $\alpha = 0.2, 0.5$ and 0.8 under different scenarios of $\sigma = 0.2, 0.4$, and 0.7 and different combinations of σ_L and σ_M while other parameters are kept as in Table 1 and σ_H is computed using the constraint in equation (9). The Figure shows the optimal distribution when Λ_α is minimized at (σ_M^*, σ_L^*) marked by red circle. First, we observe a feasible region for SD parameters, which is striped because of the implementation of two constraints in equation (9). The first constraint does not guarantee that σ_L, σ_M, and σ_H remain in interval $[0, 1]$. Therefore, we only choose the values for which $(\sigma_L, \sigma_M, \sigma_H) \in [0, 1]^3$. The optimization parameter α has an impact on $(\sigma_L^*, \sigma_M^*, \sigma_H^*)$; for small α -which is when reducing final size dominates reducing infection inequality- the lowest level of SD is devoted to the Low-income group while Middle- and High-income groups share the SD. However, when the importance of reducing infection inequality increases (α increases), the discrepancy of the level of SD among different groups decreases; that is, all groups should share SD. This discrepancy of the level of SD among different groups also decreases by increasing the SD level σ; As σ increases all σ_i^*s for

Table 2: The optimal values $(\sigma_L^*, \sigma_M^*, \sigma_H^*)$ for different values of weight α and social distancing σ. All the values are rounded up to three digits.

	$\alpha = 0.2$	$\alpha = 0.4$	$\alpha = 0.5$	$\alpha = 0.6$	$\alpha = 0.8$
$\sigma = 0.2$	(0.002, 0.335, 0.999)	(0.231, 0.196, 0.00)	(0.231, 0.193, 0.00)	(0.235, 0.192, 0.00)	(0.239, 0.183, 0.00)
$\sigma = 0.4$	(0.019, 0.875, 0.99)	(0.444, 0.383, 0.165)	(0.444, 0.383, 0.162)	(0.446, 0.382, 0.162)	(0.448, 0.380, 0.159)
$\sigma = 0.7$	(0.544, 0.877, 0.999)	(0.722, 0.691, 0.584)	(0.722, 0.691, 0.584)	(0.722, 0.691, 0.584)	(0.723, 0.693, 0.583)

$i \in \{L, M, H\}$ increase but the optimal point $(\sigma_L^*, \sigma_M^*, \sigma_H^*)$ stays on a straight line, meaning that the trend remains the same as σ changes. In the Table 2 we listed the optimal distribution $(\sigma_L^*, \sigma_M^*, \sigma_H^*)$ for various α and σ values.

In Figure 3, we plotted the time series of both the total fraction of infected cases (left panel) and infection inequality (right panel) for two scenarios of Equal Share of SD (ESD: SD implementation of an individual does not depend on his/her group), and Optimized Share of SD (OSD: when SD is distributed among groups such that $\Lambda_{0.5}$ is minimized), and for three level of low SD, $\sigma = 0.2$, medium SD, $\sigma = 0.4$ and high SD, $\sigma = 0.7$. The plots and x- and y-axis for low and medium levels of SD $\sigma = 0.2, 0.4$ are in black, while the plots and x- and y-axis for high levels of SD $\sigma = 0.7$ are in blue. The values of $(\sigma_L, \sigma_M, \sigma_H)$ for ESD are the optimized solutions listed in the third column of Table 2, $\alpha = 0.5$. While there is no significant discrepancy between ESD and OSD in the time series of infection fraction, within the OSD scenario, infection inequality is significantly smaller than that of the ESD scenario.

Figures 2, 4, and 5 take into account the variations in σ_L and σ_M but not σ_H. This is because the results of the model are not significantly affected by σ_H as the proportion of the number of contacts for the high-income-level group is only 9%. In Figures 4 and 5, we show the optimized distribution of SD, $(\sigma_L^*, \sigma_M^*, \sigma_H^*)$, versus contact levels for Low- and Middle-income groups, C_L and C_M, for $\sigma = 0.2$, Figure 4, and $\sigma = 0.4$, Figure 5. For the contact ranges we choose baseline values ± 3, thus $C_L \in [10, 15]$ and $C_M \in [7, 13]$. Then choosing the pair (C_L, C_M) in domain $[10, 15] \times [7, 13]$ and for given SD level σ, we detected the best triple $(\sigma_L^*, \sigma_M^*, \sigma_H^*)$ that minimizes $\Lambda_{0.5}$. Then we plotted each component of this triple in separate panels in Figures 4 and 5.

The *Strategy detection plot*, shown in the bottom right panel, is the combination of the other three plots in Figures 4 and 5. This plot helps us detect the optimized SD distribution given SD level σ and the number of contacts for Low- and Middle-income groups, C_L and C_M. We specify the color red for when the best strategy is that only Low-income individuals practice SD, that is, $\sigma_M^* = \sigma_H^* = 0$. Similarly, we specify the color green for when the best strategy is that only Middle-income individuals practice SD, that is, $\sigma_L^* = \sigma_H^* = 0$. Finally, we use the color blue when the best strategy is that only High-income individuals practice SD, that is, $\sigma_L^* = \sigma_M^* = 0$. Then for every pair of points (C_L, C_M) we find the best strategy $(\sigma_L^*, \sigma_M^*, \sigma_H^*)$ and then define $\sigma^* = \sigma_L^* + \sigma_M^* + \sigma_H^*$ and color that point using RGB color code $(\frac{\sigma_L^*}{\sigma^*}, \frac{\sigma_M^*}{\sigma^*}, \frac{\sigma_H^*}{\sigma^*})$ in MATLAB. The Strategy detection plot is helpful to visually detect the best strategy to control Λ_α when the resource for SD implementation is limited- for small values of σ. Therefore, we only simulated the heatmap of optimized SD parameters along with their strategy detection plot for $\sigma = 0.2$ and $\sigma = 0.4$, shown in Figures 4 and 5.

As we observe in Figures 4 and 5, the best strategy is highly dependent on the level of SD σ and contact levels C_L and C_M. For instance, when $\sigma = 0.2$ High-income group does not practice SD for almost all regions (when the contact level of the High-income group is smaller than the contact level of at least one of the other groups) or practices it highly for a small region of $C_L \sim 10$ and $C_M \in [8, 10]$ (when contact level for all groups are almost equal). On the other hand, we observe that when the contact level of a group (Low- or Middle-income) increases, then its share of optimized SD increases, which is an intuitive result of our model. Nevertheless, the striking result is that the speed of increasing σ_M^* as the contact for the Middle-income group increases is much smaller than that of Low-income ones; $\frac{d\sigma_M^*}{dC_M} < \frac{d\sigma_L^*}{dC_L}$, that is, the result is more sensitive toward behavior of Low-income group than Middle-income one. As the strategy detection plot shows, the share of color for almost all regions ($C_L \geq 11$ and $C_M \geq 10$) is between red (representing the Low-income group) and green (representing the Middle-income group). The intensity of the red color increases (decreases) as C_L increases (decreases), while the intensity of the green color increases (decreases) as C_M increases (decreases). That means the share of SD between Low- and Middle-income groups is proportional to their contact level. Increasing the SD level to $\sigma = 0.4$, we observe a completely different strategy. Looking at the strategy detection plot, we observe several points. First, the trend of increasing σ_i^* as a function of C_i for i equal to the Low- or Middle-income group is not observed for $\sigma = 0.4$; there is a complete non-linear relation between C_i and σ_i^*, that means, other factors besides the sole contact level come to play a role. Second, for a much bigger region, there is an almost equal share of SD among all groups (a gray area). Finally, for a higher level of contact for the Low-income group ($C_L \geq 12$) and a lower level of contact for the Middle-income group ($C_M \leq 10$), a share of SD among Low- and High-income groups (purple area) occurs, while the contact level for High-income group remains negligible. But when C_M increases, this share of SD moves between Low- and Middle-income groups, bigger C_M higher share of SD for the Middle-income group.

It is challenging to understand the reasons for the partitioned strategy. Many factors, such as population sizes, the contact

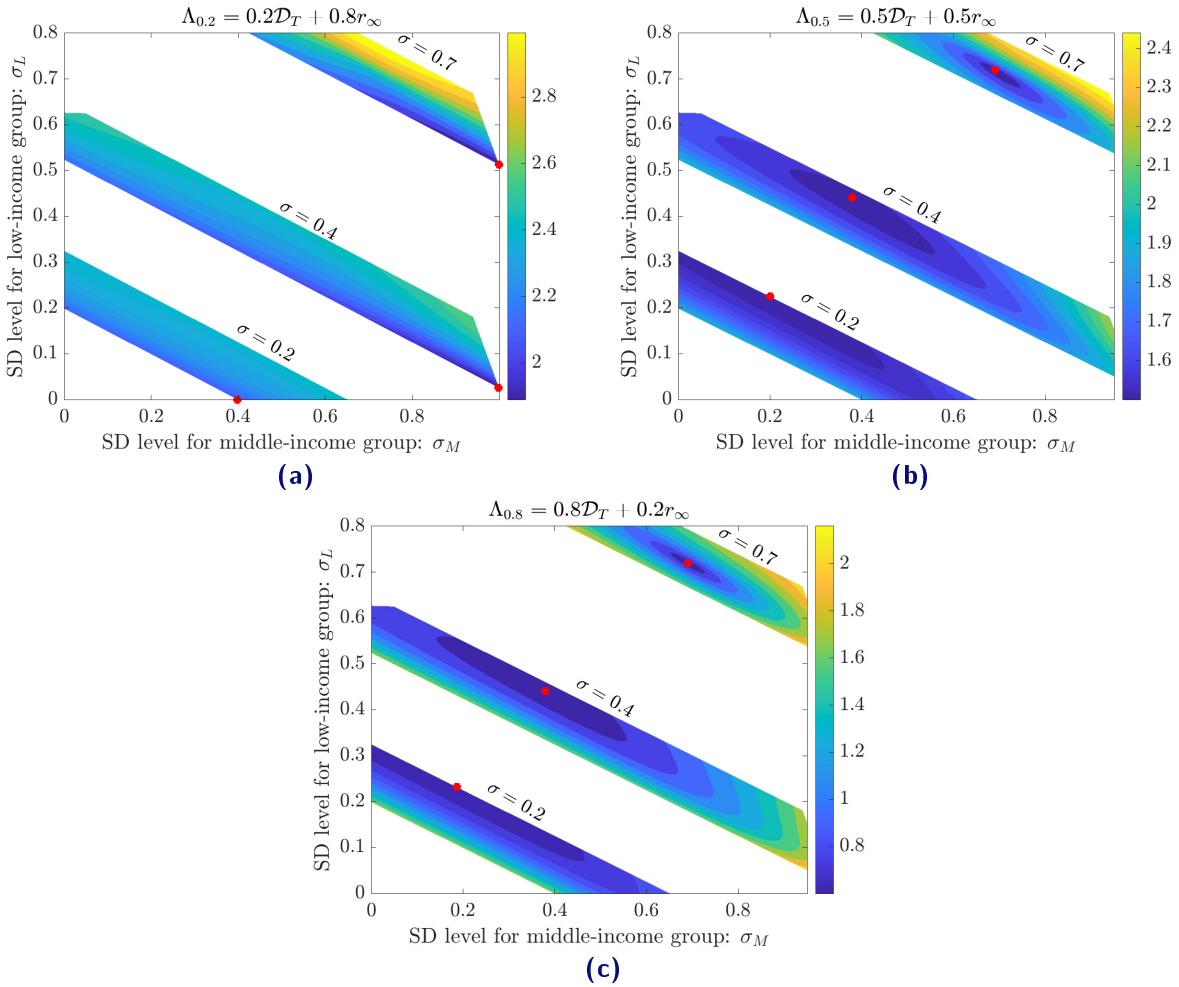

Figure 2: Sensitivity of Λ_α against two SD parameters: σ_M (x-axis) and σ_L (y-axis) for $\alpha = 0.2$ (a), $\alpha = 0.5$ (b), and $\alpha = 0.8$ (c), and $\sigma = 0.2, 0.4$, and 0.7 specified in the subfigures. Each scenario's optimum points (σ_M^*, σ_L^*) is marked as a red-filled circle.

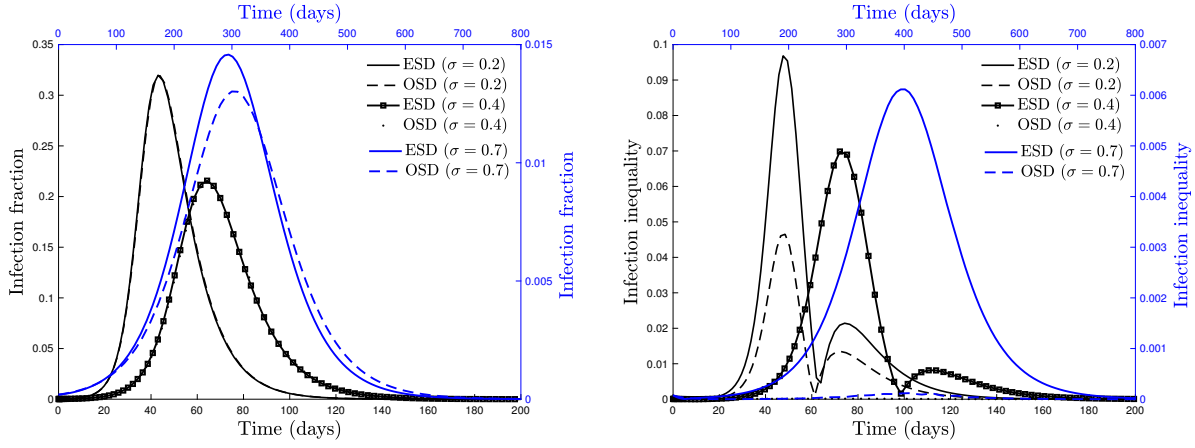

Figure 3: Time-series of infection fraction (Left panel) and infection inequality (Right panel) for scenarios of Equal share of SD (ESD) and Optimized SD (OSD) and various levels of SD $\sigma = 0.2, 0.4$ and 0.7. The black curves (refer to $\sigma = 0.2, 0.4$) are measured by the left and bottom axis specified by black color, and the blue ones (refer to $\sigma = 0.7$) are measured by the right and top axis defined by blue color.

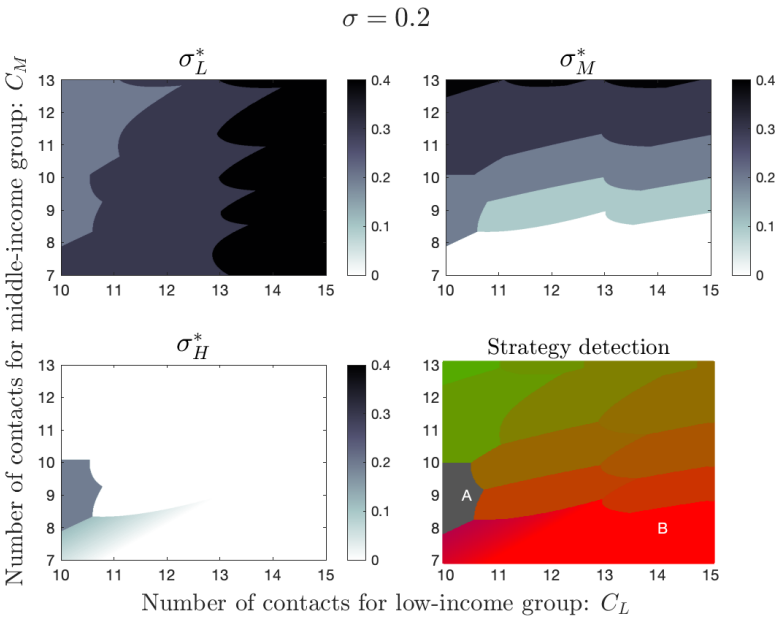

Figure 4: Optimal strategy versus contact levels for low- and Middle-income groups for $\sigma = 0.2$; The elements of optimized SD distribution $(\sigma_L^*, \sigma_M^*, \sigma_H^*)$ versus contact level for Low-income group (C_L in x-axis) and contact level for Middle-income group (C_M in the y-axis) are shown in top panels and bottom left panel. The strategy detection panel (bottom right) combines all three plots by representing each with a different primary color—red for σ_L^*, green for σ_M^* and blue for σ_H^*. For example, for point A $(C_L, C_M) = (10.5, 9)$ the first three figures indicate that $(\sigma_L^*, \sigma_M^*, \sigma_H^*) = (0.2, 0.2, 0.2)$. As a result, point A is colored gray on the strategy panel, as all primary colors are represented equally. On the other hand, for point B $(C_L, C_M) = (14, 8)$ we have $(\sigma_L^*, \sigma_M^*, \sigma_H^*) = (1, 0, 0)$. Point A is colored red on the strategy panel, as blue and green have no representation $(\sigma_M^* = \sigma_H^* = 0)$. The strategy panel clearly outlines the regions where a certain SD effort strategy provides the best outcome.

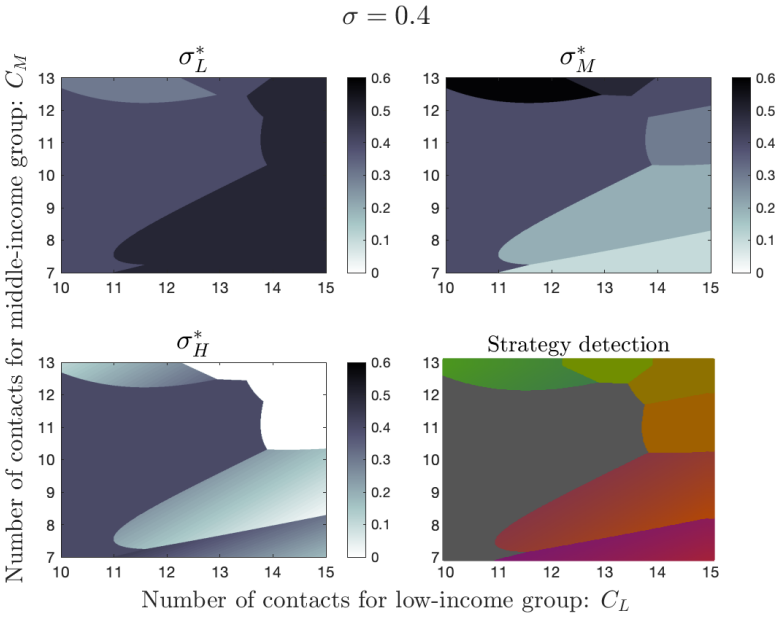

Figure 5: Optimal strategy versus contact levels for low- and Middle-income groups for $\sigma = 0.4$; The elements of optimized SD distribution $(\sigma_L^*, \sigma_M^*, \sigma_H^*)$ versus contact level for Low-income group (C_L in x-axis) and contact level for Middle-income group (C_M in the y-axis) are shown in top panels and bottom left panel. The strategy detection panel (bottom right) combines all three plots by representing each with a different primary color—red for σ_L^*, green for σ_M^* and blue for σ_H^*. Two examples are provided in the caption of Figure 4.

levels between each group (elements of matrix C), the total budget for mandated SD (σ in this context), and even the objective of SD (α in this context) can affect the best decision. However, such strategy detection plots are useful for finding the decision region.

4 Discussion and Conclusion

The disparity in infection incidence and prevalence among individuals with various socioeconomic statuses directly relates to individuals' decisions during the outbreak. These decisions depend on multiple factors primarily related to the income/education of those making them (Azizi et al., 2020). Therefore, one the main factor in controlling the infection discrepancy is managing the decisions in responding to outbreaks. One way of this management is to use an engineered mandated (public) social distancing according to socioeconomic status. To implement such social distancing, we developed a group-based mathematical model with a SIR structure to simulate emerging infection in K connected socioeconomic groups. Then, we assessed the role of mandated social distancing distribution among the groups in controlling infection inequalities and the final epidemic size. The data for our multi-objective model was from a real-world synthetic social network of individuals living in New Orleans, Louisiana. This population is proper for our study because it suffers from high health disparity rates during the COVID-19 outbreak (Louisiana Department of Health, 2020).

Our model suggested that proper social distancing management could be an effective factor for reducing the differences in infection epidemiology among socioeconomic groups, see Figure 3. Furthermore, the results suggest that the efficiency of social distancing distribution on infection inequalities reduction highly depends on the level of social distancing for all population, denoted by σ, as well as the activity level of the groups. Because when we slightly change the social distancing level or contact level for some groups, the optimum strategy changes drastically, see Figures 4 and 5.

One main point of this work is that individuals voluntarily respond to an emerging infection by considering many factors, such as fear or risk of infection and economic factors. If policies designed to control infection interfere with selective choices, it may cause unfavorable results (Azizi et al., 2022; Lee et al., 2010; Maharaj and Kleczkowski, 2012). Therefore, it is crucial to consider individuals' decisions when making mandated policies such as lock-down. One central question is how such a strategy can be implemented in reality, as it is not feasible to implement different mandated NPIs individually. However, our social network data shows that there is a homophily (McPherson et al., 2001) in socioeconomic status; people are more prone to have physical contact with others with similar socioeconomic status. One reason is their closer physical proximity, see Figure 1. Therefore, by implementing a region-based (or community-based) (Bhoi et al., 2021) mandated social distancing, we will be able to, indirectly, implement socioeconomic-based social distancing.

The proposed model, like any other mathematical modeling study, has the luxury of experimenting with social issues in a virtual environment while attempting to imitate a real-world situation (Mago et al., 2013). One of the limitations of this work is ignoring detailed information in the data such as type or time of contacts when generating contact matrix C. We only assumed a contact is a person, not a time $\times$ person. Using all this detailed information could be helpful when developing an agent-based model, which can be the direction of future work. We also ignored other social factors besides income, which may impact socioeconomic status, factors such as race and education level. Further, we have yet to consider other commonly practiced NPI or Pharmaceutical Intervention (PI), such as isolation, vaccination, and treatment in our model. Including such intervention besides behavioral change may affect the result. The other limitation of this work is incorporating only mandated SD, which the government rules and individuals must follow. This assumption and limited source of ordering SD caused the forced behavioral change of the individuals to be interdependent; that is, if a group practices a low level of SD, the others have to practice a high level of SD. In reality, individuals follow many other types of SD independent of what others do, non-mandatory self-regulated SD, which we did not consider here. In future work, we will study this effect and will measure the impact of such SDs on the efficiency of the mandated SD proposed in this work. Finally, to have a more realistic representation of our model, we need to analyze its dynamics under a limited budget scenario; that is, we need to consider the cost of selecting one strategy over the others. For example, suppose the cost of social distancing distribution among groups to control infection inequality is too high to afford. In that case, we must update the strategy for the most effective combination.

For future work, we will extend our model to an agent-based network model that can improve our assumptions, such as contact, social factors, and behavior characterized by income level, ethnicity, social groups, education level, and geographic location. We will focus on validating the model predictions and identifying which trends and quantities we can or cannot predict within the model uncertainty limitations. We will also include each strategy's cost and conduct a cost-benefit and cost-effectiveness analysis to evaluate each strategy's social or economic analysis.

It is not possible to fully capture all the micro-level social interactions leading to infection inequality. However, the present study aims to capture critical population-level average social and environmental influences and their impact on the dynamics of emerging infection and infection inequality. Although the model is still simplistic in directly guiding policymakers to alleviate this social issue, and it does not intend to do so, the qualitative trends predicted by our simulations can help design studies to quantify the effectiveness of the proposed social distancing management.

References

Álvarez, J. L., A. E. Kunst, M. Leinsalu, M. Bopp, B. H. Strand, G. Menvielle, O. Lundberg, P. Martikainen, P. Deboosere, R. Kalediene, et al. (2011). Educational inequalities in tuberculosis mortality in sixteen European populations. *The International journal of tuberculosis and lung disease 15*(11), 1461–1468. 149

Anderson, G., J. W. Frank, C. D. Naylor, W. Wodchis, and P. Feng (2020). Using socioeconomics to counter health disparities arising from the COVID-19 pandemic. *BMJ 369*. 149

Arino, J., F. Brauer, P. van den Driessche, J. Watmough, and J. Wu (2007). A final size relation for epidemic models. *Mathematical Biosciences & Engineering 4*(2), 159. 152

Azizi, A. (2023). New Orleans Social Network. `https://github.com/SoodehAzizi465051/New-Orleans-Social-Network.git`. 150, 154

Azizi, A., C. Kazanci, N. L. Komarova, and D. Wodarz (2022). Effect of human behavior on the evolution of viral strains during an epidemic. *Bulletin of Mathematical Biology 84*(12), 1–33. 150, 160

Azizi, A., C. Montalvo, B. Espinoza, Y. Kang, and C. Castillo-Chavez (2020). Epidemics on networks: Reducing disease transmission using health emergency declarations and peer communication. *Infectious Disease Modelling 5*, 12–22. 150, 160

Azizi, A., L. Xue, and J. M. Hyman (2016). A multi-risk model for understanding the spread of chlamydia. In *Mathematical and statistical modeling for emerging and Re-emerging infectious diseases*, pp. 249–268. Springer. 150

Bayham, J., N. V. Kuminoff, Q. Gunn, and E. P. Fenichel (2015). Measured voluntary avoidance behaviour during the 2009 A/H1N1 epidemic. *Proceedings of the Royal Society B: Biological Sciences 282*(1818), 20150814. 149

Bhoi, S. K., K. K. Jena, D. Mohapatra, M. Singh, R. Kumar, and H. V. Long (2021). Communicable disease pandemic: a simulation model based on community transmission and social distancing. *Soft Computing*, 1–11. 160

Block, P., M. Hoffman, I. J. Raabe, J. B. Dowd, C. Rahal, R. Kashyap, and M. C. Mills (2020). Social network-based distancing strategies to flatten the COVID-19 curve in a post-lockdown world. *Nature Human Behaviour*, 1–9. 149

Blumenshine, P., A. Reingold, S. Egerter, R. Mockenhaupt, P. Braveman, and J. Marks (2008). Pandemic influenza planning in the United States from a health disparities perspective. *Emerging infectious diseases 14*(5), 709. 149

Cao, Z., Q. Zhang, X. Lu, D. Pfeiffer, Z. Jia, H. Song, and D. D. Zeng (2020). Estimating the effective reproduction number of the 2019-nCoV in China. *MedRxiv*, 2020–01. 156

Cardoso, M. R. A., S. N. Cousens, L. F. de Góes Siqueira, F. M. Alves, and L. A. V. D'Angelo (2004). Crowding: risk factor or protective factor for lower respiratory disease in young children? *BMC Public Health 4*(1), 1–8. 149

Clouston, S. A., G. Natale, and B. G. Link (2021). Socioeconomic inequalities in the spread of coronavirus-19 in the United States: An examination of the emergence of social inequalities. *Social Science & Medicine 268*, 113554. 150

Del Valle, S., H. Hethcote, J. M. Hyman, and C. Castillo-Chavez (2005). Effects of behavioral changes in a smallpox attack model. *Mathematical biosciences 195*(2), 228–251. 149

Del Valle, S. Y., J. M. Hyman, H. W. Hethcote, and S. G. Eubank (2007). Mixing patterns between age groups in social networks. *Social Networks 29*(4), 539–554. 149

Desclaux, A., D. Badji, A. G. Ndione, and K. Sow (2017). Accepted monitoring or endured quarantine? Ebola contacts' perceptions in Senegal. *Social science & medicine 178*, 38–45. 149

Diekmann, O., J. Heesterbeek, and M. G. Roberts (2010). The construction of next-generation matrices for compartmental epidemic models. *Journal of the royal society interface 7*(47), 873–885. 152

Eubank, S. (2008). Synthetic data products for societal infrastructures and protopopulations: Data set 2.0. Technical report, Technical Report NDSSL-TR-07-003, Network Dynamics and Simulation Science. 150, 154

Eubank, S., C. Barrett, R. Beckman, K. Bisset, L. Durbeck, C. Kuhlman, B. Lewis, A. Marathe, M. Marathe, and P. Stretz (2010). Detail in network models of epidemiology: are we there yet? *Journal of biological dynamics 4*(5), 446–455. 150, 154

Farmer, P. (1996). Social inequalities and emerging infectious diseases. *Emerging infectious diseases 2*(4), 259. 149

Glass, R. J., L. M. Glass, W. E. Beyeler, and H. J. Min (2006). Targeted social distancing designs for pandemic influenza. *Emerging infectious diseases 12*(11), 1671. 153

Hartemink, N., S. Randolph, S. Davis, and J. Heesterbeek (2008). The basic reproduction number for complex disease systems: Defining R0 for tick-borne infections. *The American Naturalist 171*(6), 743–754. 152

Hyman, J. M. and J. Li (1997a). Behavior changes in SIS STD models with selective mixing. *SIAM Journal on Applied Mathematics 57*(4), 1082–1094. 149

Hyman, J. M. and J. Li (1997b). Disease transmission models with biased partnership selection. *Applied Numerical Mathematics 24*(2-3), 379–392. 149

Hyman, J. M., J. Li, and E. A. Stanley (1999). The differential infectivity and staged progression models for the transmission of HIV. *Mathematical biosciences 155*(2), 77–109. 149

Hyman, J. M., J. Li, and E. A. Stanley (2001). The initialization and sensitivity of multigroup models for the transmission of HIV. *Journal of theoretical Biology 208*(2), 227–249. 149

Jacquez, J. A., C. P. Simon, J. Koopman, L. Sattenspiel, and T. Perry (1988). Modeling and analyzing HIV transmission: the effect of contact patterns. *Mathematical Biosciences 92*(2), 119–199. 150

Kamis, C., A. Stolte, J. S. West, S. H. Fishman, T. Brown, T. Brown, and H. R. Farmer (2021). Overcrowding and COVID-19 mortality across US counties: Are disparities growing over time? *SSM-population health 15*, 100845. 150

Keeling, M. J., T. D. Hollingsworth, and J. M. Read (2020). The efficacy of contact tracing for the containment of the 2019 novel coronavirus (COVID-19). *medRxiv*. 154

Komarova, N. L., A. Azizi, and D. Wodarz (2021). Network models and the interpretation of prolonged infection plateaus in the COVID-19 pandemic. *Epidemics 35*, 100463. 150

Lee, B. Y., S. T. Brown, P. Cooley, M. A. Potter, W. D. Wheaton, R. E. Voorhees, S. Stebbins, J. J. Grefenstette, S. M. Zimmer, R. Zimmerman, et al. (2010). Simulating school closure strategies to mitigate an influenza epidemic. *Journal of public health management and practice: JPHMP 16*(3), 252. 150, 160

Leo, Y., E. Fleury, J. I. Alvarez-Hamelin, C. Sarraute, and M. Karsai (2016). Socioeconomic correlations and stratification in social-communication networks. *Journal of The Royal Society Interface 13*(125), 20160598. 156

Louisiana Department of Health (2020). COVID-19. `https://ldh.la.gov/coronavirus/`. 160

Mackenbach, J. P., I. Stirbu, A.-J. R. Roskam, M. M. Schaap, G. Menvielle, M. Leinsalu, and A. E. Kunst (2008). Socioeconomic inequalities in health in 22 European countries. *New England journal of medicine 358*(23), 2468–2481. 149

Mago, V. K., H. K. Morden, C. Fritz, T. Wu, S. Namazi, P. Geranmayeh, R. Chattopadhyay, and V. Dabbaghian (2013). Analyzing the impact of social factors on homelessness: a fuzzy cognitive map approach. *BMC medical informatics and decision making 13*(1), 94. 160

Maharaj, S. and A. Kleczkowski (2012). Controlling epidemic spread by social distancing: Do it well or not at all. *BMC public health 12*(1), 1–16. 150, 160

McPherson, M., L. Smith-Lovin, and J. M. Cook (2001). Birds of a feather: Homophily in social networks. *Annual review of sociology*, 415–444. 160

Nold, A. (1980). Heterogeneity in disease-transmission modeling. *Mathematical biosciences 52*(3-4), 227–240. 150

Quinn, S. C. and S. Kumar (2014). Health inequalities and infectious disease epidemics: a challenge for global health security. *Biosecurity and bioterrorism: biodefense strategy, practice, and science 12*(5), 263–273. 149

Snider, S. and E. Kerr (2023). Where do I fall in the American economic class system? `https://money.usnews.com/money/personal-finance/family-finance/articles/where-do-i-fall-in-the-american-economic-class-system`. 154

Sweeney, S., T. P. J. Capeding, R. Eggo, M. Huda, M. Jit, D. Mudzengi, N. R. Naylor, S. Procter, M. Quaife, L. Serebryakova, et al. (2021). Exploring equity in health and poverty impacts of control measures for SARS-CoV-2 in six countries. *BMJ global health 6*(5), e005521. 150

Sydenstricker, E. (1931). The incidence of influenza among persons of different economic status during the epidemic of 1918. *Public Health Reports (1896-1970)*, 154–170. 149

Tang, B., X. Wang, Q. Li, N. L. Bragazzi, S. Tang, Y. Xiao, and J. Wu (2020). Estimation of the transmission risk of the 2019-nCoV and its implication for public health interventions. *Journal of clinical medicine 9*(2), 462. 156

Tjepkema, M., R. Wilkins, and A. Long (2013). Socio-economic inequalities in cause-specific mortality: a 16-year follow-up study. *Canadian Journal of Public Health 104*(7), e472–e478. 149

Uscher-Pines, L., P. S. Duggan, J. P. Garron, R. A. Karron, and R. R. Faden (2007). Planning for an influenza pandemic: social justice and disadvantaged groups. *Hastings Center Report*, 32–39. 149

Valdez, L., P. A. Macri, and L. A. Braunstein (2012). Intermittent social distancing strategy for epidemic control. *Physical Review E 85*(3), 036108. 153

Van den Driessche, P. and J. Watmough (2002). Reproduction numbers and sub-threshold endemic equilibria for compartmental models of disease transmission. *Mathematical biosciences 180*(1-2), 29–48. 152

VoPham, T., M. D. Weaver, G. Adamkiewicz, and J. E. Hart (2021). Social distancing associations with COVID-19 infection and mortality are modified by crowding and socioeconomic status. *International Journal of Environmental Research and Public Health 18*(9), 4680. 149

Yang, H. M., L. P. Lombardi Junior, F. F. M. Castro, and A. C. Yang (2021). Mathematical modeling of the transmission of SARS-CoV-2—evaluating the impact of isolation in São Paulo State (Brazil) and lockdown in Spain associated with protective measures on the epidemic of COVID-19. *PLoS One 16*(6), e0252271. 156

Zelner, J., N. B. Masters, R. Naraharisetti, S. A. Mojola, M. Chowkwanyun, and R. Malosh (2022). There are no equal opportunity infectors: epidemiological modelers must rethink our approach to inequality in infection risk. *PLoS computational biology 18*(2), e1009795. 150

Zelner, J., R. Trangucci, R. Naraharisetti, A. Cao, R. Malosh, K. Broen, N. Masters, and P. Delamater (2021). Racial disparities in coronavirus disease 2019 (COVID-19) mortality are driven by unequal infection risks. *Clinical Infectious Diseases 72*(5), e88–e95. 150